Kobe University Repository : Kernel

タイトル Title	KCC Analysis of a One-Dimensional System During Catastrophic Shift of the Hill Function: Douglas Tensor in the Nonequilibrium Region
著者 Author(s)	Yamasaki, Kazuhito / Yajima, Takahiro
掲載誌・巻号・ページ Citation	International Journal of Bifurcation and Chaos,30(11):2030032
刊行日 Issue date	2020-09-15
資源タイプ Resource Type	Journal Article / 学術雑誌論文
版区分 Resource Version	author
権利 Rights	Electronic version of an article published as International Journal of Bifurcation and Chaos 30, 11, 2020, 2030032. DOI: 10.1142/S0218127420300323 © World Scientific Publishing Company. http://www.worldscientific.com/worldscinet/ijbc
DOI	10.1142/S0218127420300323
JaLCDOI	
URL	http://www.lib.kobe-u.ac.jp/handle_kernel/90007548

PDF issue: 2022-08-21

KCC analysis of a one-dimensional system during catastrophic shifts of the Hill function: Douglas tensor in the non-equilibrium region

Kazuhito Yamasaki

Department of Planetology, Graduate School of Science, Kobe University, Nada, Kobe 657-8501, Japan
yk2000@kobe-u.ac.jp

Takahiro Yajima

Department of Mechanical Systems Engineering, Faculty of Engineering, Utsunomiya University,
Utsunomiya, 321-8585, Japan
yajima@cc.utsunomiya-u.ac.jp

This paper considers the stability of a one-dimensional system during a catastrophic shift described by the Hill function. Because the shifting process goes through a non-equilibrium region, we applied the theory of Kosambi, Cartan, and Chern (KCC) to analyze the stability of this region based on the differential geometrical invariants of the system. Our results showed that the Douglas tensor, one of the invariants in KCC theory, affects the robustness of the trajectory during a catastrophic shift. In this analysis, the forward and backward shifts can have different Jacobi stability structures in the non-equilibrium region. Moreover, the bifurcation curve of the catastrophic shift can be interpreted geometrically, as the solution curve in which the nonlinear connection and the deviation curvature become zero. KCC analysis also shows that even if the catastrophic pattern itself is similar, the stability structure in the non-equilibrium region is different in some cases, from the viewpoint of the Douglas tensor.

Keywords: Jacobi stability; KCC theory; catastrophic shifts; deviation curvature; nonlinear connection; differential geometry

1. Introduction

It is well known that although nonlinear systems (e.g., ecosystems) may experience gradual changes (e.g., temperature change), this can be punctuated by a sudden drastic shift to a contrasting state (e.g., a drastic change in a population) ([May, 1977; Van Nes & Scheffer, 2007; Xiang *et al.*, 2016]). In previous studies ([Scheffer *et al.*, 2001; Kéfi *et al.*, 2013; Donangelo *et al.*, 2010]), this jump phenomenon (bifurcation) is referred to as a catastrophic shift; thus, we use this term in the present paper. Catastrophe theory are introduced by R. Thom (e.g., [Thom, 2018]), and Gilmore shows a thorough analysis of catastrophe theory for scientists and engineers [Gilmore, 1981]. Since then, catastrophic shifts have been observed in various areas of research, such as the spin system in a random magnetic field [Mirollo & Strogatz, 1990], complex disease propagation [Wang & Zou, 2016], and nonlinear oscillations in the Jeffcott rotor model [Saeed & El-Gohary, 2017].

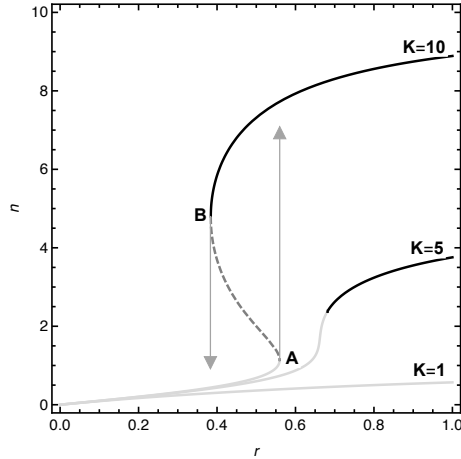As a typical example of catastrophic shifts, this paper considers the following type of ordinary differ-

Fig. 1.   Equilibrium points plotted against r for $K = 1, 5$ and 10. The light gray curve is n_a (the refuge level). The black curve is n_c (the outbreak level). The dotted curve is n_b. The catastrophic shifts occurred at points B ($r \approx 0.38$) and A ($r \approx 0.56$)

ential equation in terms of the Hill function, which has been applied to various catastrophic phenomena such as the sudden outbreak of an insect infestation (e.g., [Ludwig *et al.*, 1978; Strogatz, 2014]):

$$\frac{dn}{dt} = rn\left(1 - \frac{n}{K}\right) - \frac{n^2}{1 + n^2}, \tag{1}$$

where n is a variable, and r and K are parameters. In an ecosystem, n, r, and K correspond to the population size, growth rate, and carrying capacity, respectively. This paper uses the two parameters (growth rate r and carrying capacity K) to consider the bifurcation curve in (K, r) space of the catastrophic phenomena. Based on $dn/dt = 0$, we have four equilibrium points: $n^* = 0, n_a, n_b,$ and n_c, where $0 < n_a < n_b < n_c$. The points 0 and n_b are unstable, while n_a and n_c are stable. In an ecosystem, the smaller stable point n_a is known as the refuge level of the population, and the larger stable point n_c is the outbreak level. In this case, the unstable point n_b acts as a threshold.

The system undergoes saddle bifurcation. In ecosystems, the refuge level n_a exists for low carrying capacities (see $K = 1$ in Fig. 1). When K increases, the outbreak level n_c emerges ($K = 5$ in Fig. 1). The new feature with larger K is the unstable state n_b, which disrupts the stable states n_a and n_c ($K = 10$ in Fig. 1). The feature in a larger K is accompanied by hysteresis, or a lack of reversibility as a parameter is varied; under these circumstances, the catastrophic shift behaves as follows. Suppose we increase parameter r along the curve of $K = 10$ in Fig. 1. At point A, we see a shift from the equilibrium point to another position. If r is reduced, another shift appears at point B.

Few studies have focused on the stability of a system during catastrophic shifts, as the shifting time of catastrophes is regarded as near-instantaneous. However, catastrophic shifts in real ecosystems are not instantaneous but they take time [Scheffer et al., 2009]. For instance, when the variable n in Eq. (1) corresponds to the number of species (e.g., [Chiba, 1998; Yoshida, 2002]), the time scale of Eq. (1) is geological; thus, the catastrophic shift cannot be regarded as instant. As such, there is the possibility that some perturbations are added to the system during the shifting process.

Here, we consider system stability during catastrophic shifts, i.e., when a system shifts from one equilibrium point to another, such that the shifting process goes through a non-equilibrium region. Thus, stability analysis during a catastrophic shift should be conducted from a non-equilibrium perspective.

Recently, the theory of Kosambi, Cartan, and Chern (KCC) has received considerable attention due to its ability to characterize the stability of non-equilibrium regions (e.g., [Antonelli *et al.*, 2014; Gupta, & Yadav, 2017; Chen, & Yin, 2019]). The theory derives geometrical invariants of an ordinary differential equation, such as Eq. (1), and applies them to various systems, such as a dynamic system with bifurcations in the non-equilibrium region (e.g., [Yamasaki & Yajima, 2017]). In this study, KCC theory is applied to Eq. (1) for stability analysis during a catastrophic shift. In this application, the Douglas tensor, one

of the invariant quantities in KCC theory, is used to investigate stability in the non-equilibrium region ([Yamasaki & Yajima, 2017])

The structure of this paper is as follows. In Section 2, we provide a brief review of KCC theory. In Section 3, we provide a brief review of time-like potential in KCC theory. In Section 4, based on KCC theory, we derive the geometrical quantities of Eq. (1) and consider stability during a catastrophic shift. In Section 5, we consider climate change in terms of a catastrophic pattern similar to the one shown in Fig. 1, in which the controlling equation is not equivalent to Eq. (1). This analysis will show that the stability during the catastrophic shift differs in some cases, even if the catastrophic pattern itself is similar. Section 6 provides our conclusions.

2. KCC theory

2.1. *Basic theory*

The study of the geometric invariants of a second-order ordinary differential equation is commonly called KCC theory, i.e., the general path-space theory (e.g., [Antonelli, & Bucataru, 2003; Sabău, 2005a; Udriste & Nicola, 2009; Neagu, 2013; Harko *et al.*, 2016]). Because a dynamic system is often described by ordinary differential equations, KCC theory has been applied to the geometric aspects of various dynamic systems, including those for high-energy physics (e.g., [Lake & Harko, 2016; Dănilă *et al.*, 2016]) and biological populations (e.g., [Sabău, 2005b; Yamasaki & Yajima, 2013]). In this section, we provide a brief review of KCC theory, as it relates to catastrophic shifts.

Let us consider the path equation

$$\ddot{x}^i + g^i(x, \dot{x}) = 0, \tag{2}$$

where $g^i(x, \dot{x})$ is a smooth function. According to KCC theory (e.g., [Antonelli, & Bucataru, 2003]), a small perturbation in the trajectory of (2) gives the covariant form of the variational equation:

$$\frac{D^2 u^i}{Dt^2} = P^i_j u^j, \tag{3}$$

where $D(\cdots)/Dt$ is a covariant differential and the initial conditions are given by $u(0) = 0$ and $\dot{u}(0) \neq 0$. P^i_j is the geometric object, called the deviation curvature tensor, defined by the following relation:

$$P^i_j = -\frac{\partial g^i}{\partial x^j} + \frac{\partial N^i_j}{\partial x^k} \dot{x}^k - G^i_{jk} g^k + N^i_k N^k_j, \tag{4}$$

N^i_j is a coefficient related to the nonlinear connection:

$$N^i_j = \frac{1}{2} \frac{\partial g^i}{\partial \dot{x}^j}, \tag{5}$$

and G^i_{jk} is a Berwald connection:

$$G^i_{jk} = \frac{\partial N^i_j}{\partial \dot{x}^k}. \tag{6}$$

Here, we consider the deviation curvature, which is an invariant quantity in KCC theory. According to previous studies, there are other invariant quantities in KCC theory: the torsion tensor Q^i_{jk}, the Riemann–Christoffel curvature tensor R^i_{jkl}, and the Douglas tensor D^i_{jkl} ([Douglas, 1927; Antonelli, & Bucataru, 2003]). They are defined as

$$Q^i_{jk} = \frac{1}{3} \left(\frac{\partial P^i_j}{\partial \dot{x}^k} - \frac{\partial P^i_k}{\partial \dot{x}^j} \right), \tag{7}$$
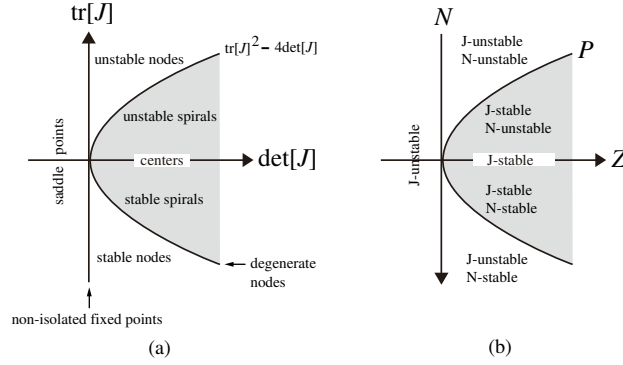
Fig. 2.   Type and stability of the equilibrium points (modified from [Yamasaki & Yajima, 2013]). (a) The well-known diagram is expressed in terms of a Jacobian J of the linearized system around the equilibrium points. (b) The corresponding diagram is expressed in terms of the geometrical quantities based on the theory presented by Kosambi, Cartan, and Chern (KCC theory). Note that the N-axis is reversed. From [Yamasaki & Yajima, 2013], $N = -(1/2)\mathrm{tr}[J]$, $Z = \det[J]$ and $P = N^2 - Z$.

$$R^i_{jkl} = \frac{\partial Q^i_{jk}}{\partial \dot{x}^l}, \tag{8}$$

$$D^i_{jkl} = \frac{\partial G^i_{jk}}{\partial \dot{x}^l}. \tag{9}$$

In previous analyses, the Douglas tensor was not considered because the function D^i_{jkl} often takes a zero value. In catastrophic shifts, the function D^i_{jkl} can take a nonzero value, so we consider it here. Other functions, such as Q^i_{jk} and R^i_{jkl}, are not defined in a one-dimensional system, so we do not consider them. As will be shown, the Douglas tensor controls stability during catastrophic shifts, i.e., in the non-equilibrium region.

As the one-dimensional case is considered here, we set $n^1 = n$, $x^1 = x$, $g^1 = g$, $G^1_{11} = G$, $N^1_1 = N$, and $P^1_{11} = P$ for simplicity.

2.2.   *J-stability and N-stability*

It is known that the deviation curvature (4) is closely related to the Jacobi stability. The Jacobi stability can be taken to represent the robustness of the whole trajectory of a system, in terms of small perturbations [Lake & Harko, 2016; Sabău, 2005a]. According to previous studies [Antonelli, & Bucataru, 2003; Sabău, 2005a,b], the trajectories of a one-dimensional system are Jacobi-stable when $P < 0$, and Jacobi-unstable when $P \geq 0$. In this paper, we refer to the system as J-stable when $P < 0$, and as J-unstable when $P \geq 0$. Around the equilibrium points, J-stable and J-unstable correspond to a spiral and a node, respectively (e.g., [Sabău, 2005b; Yamasaki & Yajima, 2013, 2016]).

Moreover, we consider the stability related to the nonlinear connection (5). In this paper, we refer to the system as being N-stable when $N > 0$, as N-unstable when $N < 0$, and as N-neutral when $N = 0$. Around the equilibrium points, N-stable, N-unstable, and N-neutral correspond to linear stable, linear unstable, and neutral, respectively [Yamasaki & Yajima, 2013, 2016]. This association has been confirmed in well-known systems, such as the prey–predator model and the two-species competition model ([Yamasaki & Yajima, 2013]).

The relationship between the stability type of bifurcation theory and the geometric terms of KCC theory around the equilibrium points is summarized in Fig. 2 [Yamasaki & Yajima, 2013] and Table 1.

In the last, we review the relationship between the stability in KCC theory and other definitions, such as Lyapunov and orbital stability. Abolghasem (2013b) reviewed the relationship between Jacobi and Lyapunov stability. Boehmer et al. (2010) analyzed the relationship between the Jacobi and linear Lyapunov stability of dynamical systems in the fields of gravitation and astrophysics, and show that there are cases in which Lyapunov and Jacobi stability do not agree. Abolghasem showed that these stability

Table 1.   Summary of the results presented in Fig. 2.

	$P > 0$	$P = 0$	$P < 0$
$N > 0$	stable nodes	degenerate nodes	stable spirals
$N = 0$	saddle	degenerate nodes	center
$N < 0$	unstable nodes	degenerate nodes	unstable spirals

concepts agree in three cases of torque-free rigid body motion around a stationary point, circular orbits in a central force field, and circular orbits in Schwarzschild spacetime ([Abolghasem, 2012a,b, 2013a]). Abolghasem (2013b) explicitly showed that the stability derived from Lyapunov analysis is the same as Jacobi stability for a Hamiltonian system with one degree of freedom. There few studies have examined the relationship between KCC theory and orbital stability, although asymptotical orbital stability is considered in predation and herbivory ecosystems ([Antonelli, & Kazarinoff, 1984]).

3.   Time-like potential of KCC theory in bifurcation

Following Antonelli's approach [Antonelli *et al.*, 1993; Yamasaki & Yajima, 2017], we introduce the concept of time-like potential x^i, defined as

$$n^i = a\dot{x}^i, \tag{10}$$

where $a(\neq 0)$ is a constant. This approach is well-suited to the study of bifurcation in dynamical systems [Yamasaki & Yajima, 2017]. Here, the deviation curvature (4) can be simplified as follows

$$P_j^i = -G_{jk}^i g^k + N_k^i N_j^k. \tag{11}$$

In the following analysis, we use (11) with (5) and (6).

3.1.   *A brief review of time-like potential in KCC theory*

The concept of time-like potential in KCC theory is utilized, as described above. Time-like potential is a complex subject, so a brief explanation of the concept is provided here. This work focuses on the jump phenomenon (bifurcation) referred to as a catastrophic shift, so time-like potential is discussed in this context in the next subsection.

The subject of KCC theory is a second-order ordinary differential equation (ODE), so KCC theory cannot be applied to a first-order ODE. Therefore, the Jacobi stability bifurcations described by first-order ODEs has not been studied. Antonelli et al., (1993) introduced the production process concept, which enables the application of KCC theory to first order ODEs such as the logistic equation (see Antonelli, 1985). Here, the logistic equation becomes the second-order ODE that has been applied to real growth data for several species ([Antonelli, 1985; Antonelli *et al.*, 1993]). Furthermore, Yamasaki and Yajima (2017) applied this technique to typical one-dimensional bifurcations described by first-order ODEs, such as saddle-node, transcritical, and pitchfork bifurcations.

The production process is described in terms of the time-like potential defined by $n = a\dot{x}$ where $a > 0$ ([Antonelli *et al.*, 1993]). For example, the variable n corresponds to the number of individuals in an ecosystem population. The population n physically exists, whereas the time-like potential x is a purely mathematical construct. The time-like potential corresponds to the time integral of the population. Therefore, this formulation has been used to study transient behaviors during the production process, such as the effects of time feedback ([Hutchinson, 1948; Wright, 1955]) and the logistics of a system in a limited environment ([Antonelli *et al.*, 1993]).

It would be appropriate to express the analytical results in terms of n, rather than in the time-like potential x. Specifically, this paper considers bifurcation stability, so it is necessary to express the geometric quantities related to stability in terms of n. As we will see in the later section, the nonlinear connection

related to N-stability given by Eq. (33), and the deviation curvature related to J-stability given by Eq. (35), are expressed in terms of n in the last step (r and K are parameters). Thus, the time-like potential can be used as part of the analytical process, but is not necessary for interpretation of the bifurcation stability.

The equation derived by the time-like potential exhibits the same bifurcation as the original equation ([Yamasaki & Yajima, 2017]). In the next subsection, we will consider this point in the context of a more general case by focusing on the bifurcation occurrence condition with respect to the geometric quantities of KCC theory.

3.2. *Bifurcation in a time-like potential system*

The catastrophic shifts considered in this paper undergo saddle-node bifurcation [Strogatz, 2014]. Therefore, it is important to consider the relationship between the bifurcation and time-like potential in KCC theory. In this subsection, we consider this point by focusing on the bifurcation occurrence condition and implement typical birfurcations, such as the saddle-node, transcritical, and pitchfork birfurcations in one-dimensional space.

First, we consider the saddle-node bifurcation, which plays an essential role in catastrophic shifts. The normal form of the saddle-node bifurcation is given by $\dot{n} + f(n, r) = 0$, where

$$f(n, r) = -r - n^2. \tag{12}$$

The saddle-node bifurcation occurrence condition at the point $x = 0$, with the bifurcation parameter $r = 0$ is given by (e.g., [Iooss, & Joseph, 1980; Komuro, 2002]):

$$f(0, 0) = \partial_n f(0, 0) = 0, \quad \partial_r f(0, 0) \neq 0, \quad \partial_n \partial_n f(0, 0) \neq 0. \tag{13}$$

Eq. (12) satisfies all the conditions (13).

Next, we consider the time-like potential of the saddle-node bifurcation. From $n = a\dot{x}$, the basic equation $\dot{n} + f(n, r) = 0$ becomes $a\ddot{x} + f(n, r) = 0$. Through comparison between this equation and the basic KCC theory equation: $\ddot{x} + g(\dot{x}, r) = 0$, we obtain $(1/a)f(n, r) = g(\dot{x}, r)$. Moreover, the differential is $\partial_{\dot{x}}(\cdots) = a\partial_n(\cdots)$. From $a > 0$, the condition $n = 0$ corresponds to $\dot{x} = 0$, so several relationships can be obtained between g and f, such as $\partial_{\dot{x}} g(0, r) = a\partial_n((1/a)f(0, r)) = \partial_n f(0, r)$. Alternatively, g leads to geometric quantities such as (5), (6), (9) and (11). Therefore, geometric quantities can be derived directly from f:

$$g = \frac{f}{a}, \tag{14}$$

$$N = \frac{1}{2}\partial_n f, \tag{15}$$

$$G = \frac{1}{2}a\partial_n\partial_n f, \tag{16}$$

$$P = -\frac{1}{2}f\partial_n\partial_n f + \frac{1}{4}(\partial_n f)^2, \tag{17}$$

$$D = \frac{1}{2}a^2\partial_n\partial_n\partial_n f. \tag{18}$$

As $n = 0$ corresponds to $\dot{x} = 0$, these relationships show that conditions written in terms of f (13) can be rewritten as conditions in terms of the geometric quantities of KCC theory:

$$g(0,0) = N(0,0) = 0, \quad \partial_r g(0,0) \neq 0, \quad G(0,0) \neq 0. \tag{19}$$

The geometric quantities of saddle-node bifurcation derived using the time-like potential are given by [Yamasaki & Yajima, 2017]:

$$g = -\frac{r}{a} - \frac{n^2}{a}, \quad N = -n, \quad G = -a. \tag{20}$$

These satisfy all of the conditions (19). That is, saddle-node bifurcation also occurs in the time-like potential system.

Next, in a similar fashion, we consider transcritical bifurcation. The normal form of the system is given by $\dot{n} + f(n,r) = 0$, where

$$f(n,r) = -rn + n^2 \tag{21}$$

The transcritical bifurcation occurrence condition is given by

$$f(0,0) = \partial_n f(0,0) = f(0,r) = \partial_r f(0,0) = 0,$$
$$\partial_n \partial_r f(0,0) \neq 0, \quad \partial_n \partial_n f(0,0) \neq 0. \tag{22}$$

From (14), (15) and (16), these conditions can be rewritten geometrically

$$g(0,0) = N(0,0) = g(0,r) = \partial_r g(0,0) = 0,$$
$$\partial_r N(0,0) \neq 0, \quad G(0,0) \neq 0. \tag{23}$$

The geometric quantities of transcritical bifurcation derived using the time-like potential are given by [Yamasaki & Yajima, 2017]:

$$g = -r\frac{n}{a} + \frac{n^2}{a}, \quad N = -\frac{1}{2}r + n, \quad G = a. \tag{24}$$

These satisfy all of the conditions (23). That is, transcritical bifurcation also occurs in the time-like potential system.

Finally, we consider pitchfork bifurcation. The normal form of the system is given by $\dot{n} + f(n,r) = 0$, where

$$f(n,r) = -rn + n^3 \tag{25}$$

The pitchfork bifurcation occurrence condition is given by

$$f(-n,r) = -f(n,r),$$
$$f(0,0) = \partial_n f(0,0) = \partial_r f(0,0) = \partial_n \partial_n f(0,0) = 0,$$
$$\partial_n \partial_r f(0,0) \neq 0, \quad \partial_n \partial_n \partial_n f(0,0) \neq 0. \tag{26}$$

From (14), (15), (16) and (18), these conditions can be rewritten geometrically:

$$g(-n,r) = -g(n,r),$$
$$g(0,0) = N(0,0) = \partial_r g(0,0) = G(0,0) = 0,$$
$$\partial_r N(0,0) \neq 0, \quad D(0,0) \neq 0. \tag{27}$$

The geometric quantities of pitchfork bifurcation derived using time-like potential are given by [Yamasaki & Yajima, 2017]:

$$g = -r\frac{n}{a} + \frac{n^3}{a}, \quad N = \frac{1}{2}(-r + 3n^2), \quad G = 3an, \quad D = 3a^2. \tag{28}$$

These satisfy the necessary conditions (27), that is, pitchfork bifurcation also occurs in the time-like potential system.

These results show that the typical bifurcation of a one-dimensional system also occurs in the time-like potential system. Therefore, this approach can be used to consider the catastrophic shifts associated with bifurcation.

4. KCC theory and catastrophic shift

4.1. *Geometrical quantities of the catastrophic shift*

In KCC theory, the stability of the system is characterized by geometrical quantities, such as the nonlinear connection and the deviation curvature. To derive these geometrical quantities of (1), this paper follows Antonelli's approach [Antonelli *et al.*, 1993; Yamasaki & Yajima, 2017], in which the time-like potential $n^i = a\dot{x}^i$ is substituted into the basic equation (1):

$$\ddot{x} + g = 0 \tag{29}$$

with

$$g = -r\dot{x} + \frac{r}{K}a\dot{x}^2 + \frac{a\dot{x}^2}{1 + (a\dot{x})^2}. \tag{30}$$

Given that the term g is given by (30), we can use Eqs. (5), (6), and (11) to obtain the differential geometrical quantities, as follows. From Eq. (5), the nonlinear connection can be derived by

$$N = \frac{1}{2}\frac{\partial g}{\partial \dot{x}} \tag{31}$$

$$= r\left(\frac{a\dot{x}}{K} - \frac{1}{2}\right) + \frac{a\dot{x}}{(1 + (a\dot{x})^2)^2} \tag{32}$$

$$= r\left(\frac{n}{K} - \frac{1}{2}\right) + \frac{n}{(1 + n^2)^2}, \tag{33}$$

where we use $n = a\dot{x}$ in the last step to express the geometrical quantity in terms of n. In a similar fashion, Eq. (6) gives the Berwald connection:

$$G = a\left(\frac{r}{K} + \frac{1 - 3n^2}{(1 + n^2)^3}\right), \tag{34}$$

and Eq. (11) gives the deviation curvature:

$$P = \frac{r^2}{4} + \frac{rn^3(3n - n^3 - 4K)}{K(1 + n^2)^3} + \frac{3n^4}{(1 + n^2)^4}. \tag{35}$$

As mentioned in Section 2.2, from the sign of the nonlinear connection and the deviation curvature, we can consider the stability in the non-equilibrium region. To obtain a visual image of this structure, we can rewrite the results of Fig. 1 as Fig. 3, in which we add the contour plots based on the geometrical quantities (33) and (35) for each carrying capacity: $K = 1$, $K = 5$, and $K = 10$.

First, we consider the left side of Fig. 3. The positive N region is N-stable. Especially around the equilibrium points, N-stable corresponds to linear stable (Fig. 2). In fact, Fig. 3 shows that the white solid line (stable equilibrium points) is always in the positive N region. On the other hand, the white dotted line (unstable equilibrium points) is in the negative N region (i.e., the N-unstable region). Next, we consider the right side of Fig. 3, which shows that the region around the equilibrium points has a positive P, i.e., J-unstable. From Fig. 2, it can be seen that this corresponds to the node-type around the equilibrium points, in agreement with the results of previous analyses (e.g., [Strogatz, 2014]).

Combining the contour plots in Fig. 3, we can draw Figs. 4 and 5, in which the areas are denoted as follows: N-unstable (negative N) and J-unstable (positive P), black; N-unstable and J-stable, white; N-stable and J-unstable, dark gray; and N-stable and J-stable, light gray. The change in the equilibrium line (white line) for each K is simple; however, the change in the non-equilibrium region (gray-scale patterns) for each K is relatively complicated. In the next section, we will see that this complicated pattern affects stability during a catastrophic shift.
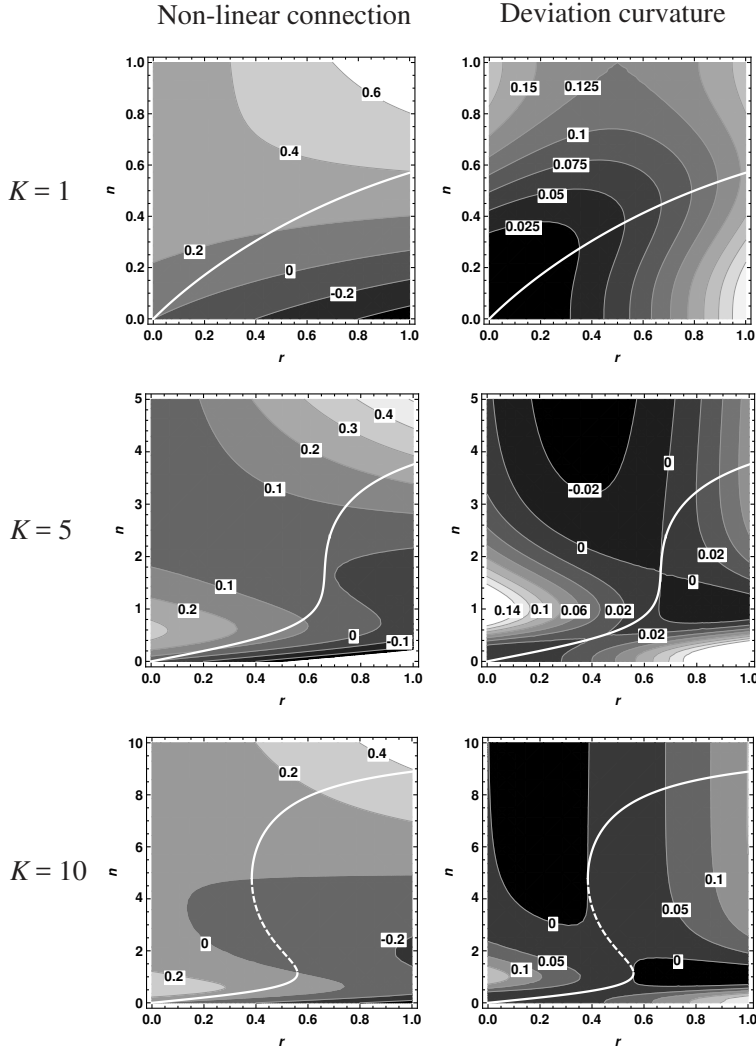
Fig. 3. Contour plots of the nonlinear connection (left) and the deviation curvature (right) for $K = 1, 5,$ and 10. The white solid and dotted lines indicate stable and unstable equilibrium lines, respectively (see Fig. 1). Note that the aspect ratio of the figures of $K = 1$ and 5 is different from that in Fig. 1.

4.2. *Stability during a catastrophic shift*

As mentioned in the Introduction, the case of $K = 10$ is accompanied by a catastrophic shift, as shown in Fig. 5. We plot the starting points as A1 and B1, and the corresponding ending points as A2 and B2. During the catastrophic shift, the system shifts from one equilibrium point (A1 or B1) to another (A2 or B2); during the shifting process, the system goes through a region of non-equilibrium.

First, we consider the J-stability of the shift from point A1 to A2. During this shift, the system goes through two stability regions, denoted in black and dark-gray in Fig. 5. Given that the sign of the deviation curvature is always positive, the system is always Jacobi unstable during the catastrophic shift. However, the starting point A1 is located near the white region (J-stable region); thus, it is expected that the degree of J-instability is smaller closer to point A1. To show this more clearly, the cross-section of the topographic profile of the catastrophic shift in Fig. 3 is shown on the left side of Fig. 6. This shows that the degree of J-instability increases toward the ending point A2. As mentioned in Section 2.2, the Jacobi stability can be taken to represent the robustness of the system trajectory [Lake & Harko, 2016; Sabău, 2005a], and the degree of Jacobi instability is inversely proportional to the value $P(> 0)$. Therefore, the left side of Fig. 6 indicates that the trajectory robustness during the catastrophic shift decreases from A1 to A2.
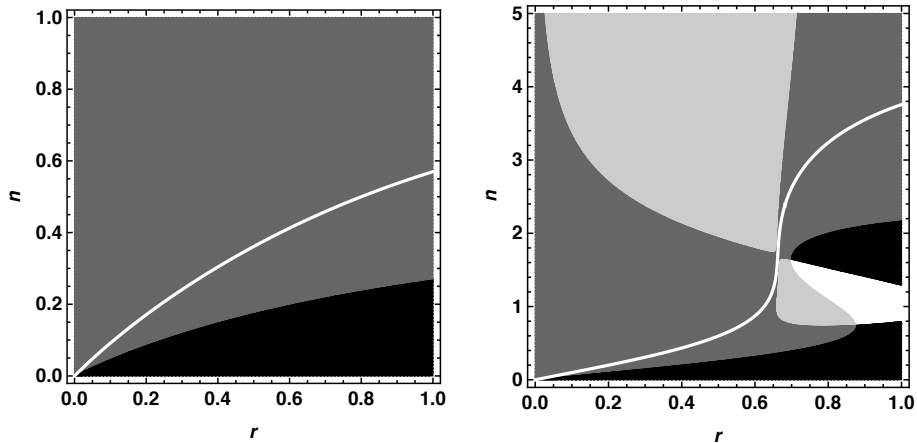
Fig. 4.   N-stability and J-stability of the system for $K = 1$ (left) and $K = 5$ (right). The white (black) region shows N-unstable and J-stable (unstable) areas. The light (dark) gray region shows N-stable and J-stable (unstable) areas.
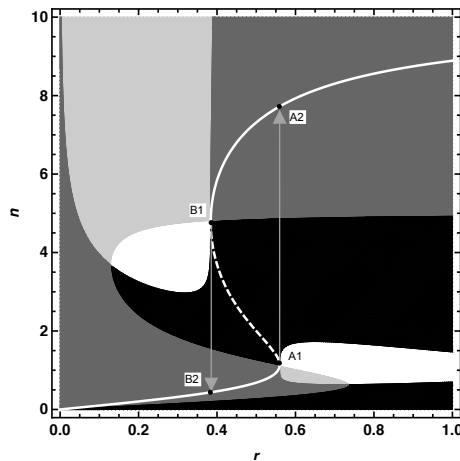

Fig. 5.   N-stability and J-stability of the system for $K = 10$. The white (black) region shows N-unstable and J-stable (unstable) areas. The light (dark) gray region shows N-stable and J-stable (unstable) areas. The jump occurs at A1 ($r \approx 0.56$, the right gray arrow line) and B1 ($r \approx 0.38$, the left gray arrow line)).
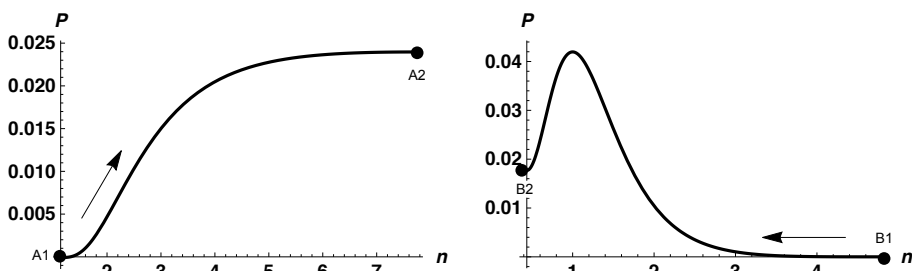

Fig. 6.   Cross-section of "the topographic profile" of the deviation curvature in $K = 10$ (Fig. 3) along the catastrophic shift. The left figure is the profile along A1 to A2 (the backward shift). The right figure is the profile along B1 to B2 (the forward shift).

Next, we consider the J-stability of the shift from point B1 to B2. In a similar fashion, we draw the cross-section from B1 to B2 (the right side of Fig. 6). This is different from the cross-section A1A2, i.e., the maximum value of the J-instability is not the ending point B2. In previous studies, this difference between the two cross-sections, A1A2 and B1B2, was not addressed. KCC theory shows that the forward

shift, B1B2 (the catastrophic shift to the lower alternative stable state), differs in trajectory robustness compared with the backward shift, A1A2 (the catastrophic shift to the upper alternative stable state).

We consider the results in Fig. 6 based on the extremum of P and the equilibrium solution of n. From Eqs. (1) and (35), we obtain

$$\frac{dP}{dn} = \frac{12}{(1+n^2)^4}(n+1)n(n-1)\frac{dn}{dt}. \tag{36}$$

This equation shows that the non-zero solutions of (1): $n_a < n_b < n_c$ also give the extremum of P. On the left side of Fig. 6 (i.e., $n > 1$), Eq. (36) shows the catastrophic shift from A1 to A2 (i.e., $dn/dt > 0$), resulting in $dP/dn > 0$. On the right side of Fig. 6, Eq. (36) shows that the catastrophic shift from B1 to B2 (i.e., $dn/dt < 0$) gives $dP/dn < 0$ for $n > 1$ and $dP/dn > 0$ for $n < 1$. From Eq. (11) with (5) and (6), the general equation between dP/dn and dn/dt is given by [Yamasaki & Yajima, 2017]

$$\frac{dP}{dn} = \frac{D}{a^2}\frac{dn}{dt}, \tag{37}$$

where D is the Douglas tensor in one-dimensional space defined by $D = a(\partial G/\partial n)$. In general, the Douglas tensor is one of the invariant quantities in KCC theory, defined by $D^i_{jkl} = a(\partial G^i_{jk}/\partial n^l)$([Douglas, 1927; Antonelli, & Bucataru, 2003]). In fact, from (34), we obtain $D/a^2 = (1/a)(\partial G/\partial n) = 12n(n^2-1)/(1+n^2)^4$, in agreement with the coefficient of Eq. (36). In previous analyses of KCC theory, the Douglas tensor had not received attention for the following two reasons: (1) the function D_{ijkl} often takes a zero value, because we considered a system that includes a lower-order term; and (2) the stability analysis was conducted around the equilibrium points. However, [Yamasaki & Yajima, 2017] suggests that the Douglas tensor is a useful invariant quantity when considering N-stability and J-stability in the non-equilibrium region. In fact, Eq. (37) shows that the sign of the Douglas tensor affects the robustness of the trajectory in the non-equilibrium region (i.e., $dn/dt \neq 0$).

Finally, we consider the large change in n in the non-catastrophic case. Enough perturbation at the fold point of the equilibrium line can also cause a significant change in n in the absence of true bifurcation (non-catastrophic shift) (e.g., Fig. b in [Scheffer et al., 2009]). In this paper, this case corresponds to the right of Fig. 4; the perturbation at the fold point causes the system to go through two stability regions, shown as light-gray and dark-gray areas. Thus, the non-catastrophic shift goes from the J-stable region to the J-unstable region. As the catastrophic shift is always J-unstable, the robustness of a non-catastrophic shift trajectory is qualitatively different from that of a catastrophic shift.

4.3. *Bifurcation curve*

The system described by Eq. (1) undergoes saddle bifurcation(e.g., [Strogatz, 2014]). The conditions for a saddle-node bifurcation in Eq. (1) give $r(1-n/K) = n/(1+n^2)$ and $(d/dn)[r(1-n/K)] = (d/dn)[n/(1+n^2)]$. From these two equations, we have

$$r = \frac{2n^3}{(n^2+1)^2} \quad \text{and} \quad K = \frac{2n^3}{n^2-1}. \tag{38}$$

These two equations give the bifurcation curve in (K, r) space. We consider the geometrical aspect of this result from the viewpoint of KCC theory.

First, we consider the boundary of the N-stability in the non-equilibrium region. When $N = 0$ in Eq. (33), we have

$$r = \frac{2Kn}{(K-2n)(1+n^2)^2}. \tag{39}$$

This equation gives the boundary between N-stable and N-unstable conditions. For instance, on the left side of Fig. 4, the boundary line between the black region (N-unstable and J-unstable) and the dark-gray region

(N-stable and J-unstable) is given by Eq. (39). Since $r > 0$ in the ecological system, the boundary line should satisfy $n < K/2$. This means that the carrying capacity K determines the limit of the N-unstable region. The boundary line of the N-stability does not necessarily correspond to the equilibrium line (the white line).

Next, we consider the boundary of J-stability. When $P = 0$ in Eq. (35), we have

$$r = \frac{2n^2}{K(n^2+1)^3}(A \pm \sqrt{B}), \tag{40}$$

with

$$A = n(n^3 - 3n + 4K), \tag{41}$$

$$B = (n^2 - 3)(n^6 - 3n^4 + 8Kn^3 - 3K^2n^2 + K^2). \tag{42}$$

This equation corresponds to the boundary between J-stable and J-unstable. In Figs. 4 and 5, the white lines are always included in the J-unstable region. This reflects the fact that the equilibrium point of Eq. (1) is node-type.

The bifurcation curve described by Eq. (38) is expected to be related to the sign of the geometrical quantities N and P. Then, we consider the simultaneous equations $N = 0$ and $P = 0$. The solutions of these equations are given by

$$\begin{cases} r = \frac{2n^3}{(n^2+1)^2} \\ K = \frac{2n^3}{n^2-1} \end{cases} \tag{43}$$

or

$$\begin{cases} r = \frac{8n^3}{(n^2+1)^3} \\ K = \frac{8n^3}{3n^2-1} \end{cases} \tag{44}$$

The solutions (43) are in agreement with the previous solutions (38). This means that the bifurcation curve can be interpreted geometrically as the solution curve in which all of the geometrical quantities, related to the stability, become zero. Notably, other solutions (44) can be obtained; however, interpretation of these solutions is beyond the scope of this paper. Further consideration of (44) will be undertaken in future works.

5.   Comparison with the results of other models: climate change

Climate change is one of the phenomena accompanied by a catastrophic shift (e.g., [Ghil, & Childress, 1987; Eisenman, & Wettlaufer, 2009; Bathiany *et al.*, 2018]). In fact, the equilibrium temperature curve of climate change, shown in Fig. 7, is folded backwards (e.g., [Li *et al.*, 1997]), similar to the white equilibrium curve of Fig. 5. Here we compare our results with those of the climate change model, from the viewpoint of KCC analysis.

The model considered in this section is the classical climate change model, or zero-dimensional energy balance model (e.g., [Budyko, 1969; Sellers, 1969; Crafoord, & Källén, 1978]):

$$C\frac{dT}{dt} = R_i - R_o, \tag{45}$$

where C is the heat capacity of the system, T is the globally averaged temperature of the Earth, R_i is the net incoming radiation, and R_o is the outgoing radiation. The functional form of R_i is given by $R_i = \mu S(1 - \alpha)/4$, where S is the solar constant, i.e., 1.37×10^3 [Wm^{-2}], and μS corresponds to present-day radiation conditions for $\mu = 1$. The parameter α is the albedo considered below. Following [Crowley, & North, 1991], the functional form of R_o is $R_o = -363 + 2.1T$. Several functional forms of the albedo α are
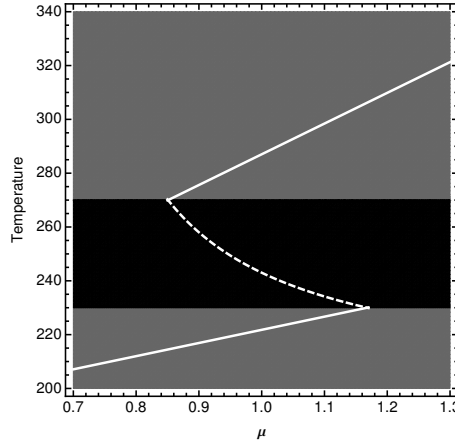
Fig. 7.   Equilibrium temperature depends on μ. The white solid and dotted lines indicate the stable and unstable equilibrium lines, respectively. The black region shows N-unstable and J-unstable areas. The dark gray region shows N-stable and J-unstable areas. The parameters are as follows: $\alpha_0 = 0.7$, $\alpha_1 = 0.3$, $T_1 = 230$, and $T_2 = 270$.

available in the literature ([Roques *et al.*, 2014]). This paper follows the Sellers-type model, a widely used model presented here as a step function ([Sellers, 1969]):

$$\alpha = \begin{cases} \alpha_0, & \text{for } T \leq T_1, \\ \alpha_0 + (\alpha_1 - \alpha_0)(T - T_1)/(T_2 - T_1), & \text{for } T_1 < T < T_2, \\ \alpha_1, & \text{for } T \geq T_2, \end{cases} \tag{46}$$

where $\alpha_0 > \alpha_1 > 0$ and $T_1 < T_2$ are all constants.

From $dT/dt = 0$, we obtain the equilibrium temperature curve shown in Fig. 7 as white solid and dotted lines. As described above, this pattern is folded backwards similar to the white equilibrium curve shown in Fig. 5. Thus, climate change in the Seller-type model also shows a catastrophic shift.

Next, KCC theory was applied to derive the geometrical invariants of Eq. (45) with Eq. (46), similar to the approach discussed in Section 3. As a result, we obtain the N-stability and J-stability shown in Fig. 7 as a gray-scale pattern. The results shown in Fig. 7 differ from those in Fig. 5, in that climate change in the Seller-type model shows an another stability structure in the non-equilibrium region. In fact, the Douglas tensor D of the model is calculated to be zero. Therefore, Eq. (37) shows that the deviation curvature is constant during the catastrophic shift, which differs from the topographic profiles shown in Fig. 6. Given that $D = \partial G/\partial \dot{x} = \partial^2 N/\partial \dot{x}^2 = (1/2)\partial^3 g/\partial \dot{x}^3$, the deviation curvature (i.e., J-stability) is not constant (i.e., $dP/dn \neq 0$) during the catastrophic shift when the system includes terms higher than second-order.

Moreover, the white area (J-stable area), seen near the bifurcation points A1 and B1 in Fig. 5, does not exist in Fig. 7. Therefore, although the perturbation is added to the system at the bifurcation point, the catastrophic process associated with climate change never goes through the J-stable region. These results imply that even if the catastrophic pattern itself is similar, the stability structure in the non-equilibrium region is different in some cases.

6.   Conclusions

Our main conclusions are as follows.

(1) In our investigation of stability during a catastrophic shift (i.e., non-equilibrium), we identified a difference between the backward shift and the forward shift. During the backward shift, the robustness of the trajectory decreases toward the upper alternative equilibrium point. During the forward shift, the robustness retains its minimum value during the catastrophic shift. The J-stability during these catastrophic shifts can be described by the following:

$$\frac{dP}{dn} = \frac{D}{a^2}\frac{dn}{dt}, \tag{47}$$

where D is the Douglas tensor. This equation means that the sign of the Douglas tensor determines the extremum of P during the backward shift ($dn/dt > 0$) and the forward shift ($dn/dt < 0$).

(2) In KCC analysis, the bifurcation curve can be interpreted geometrically as the solution curve, in which the nonlinear connection and the deviation curvature become zero.

(3) This paper considers mainly the catastrophic model often used to describe the ecosystem. We compared the model with other catastrophic models often used to describe climate change, to show that even if the catastrophic pattern itself is similar, the stability structure in the non-equilibrium region is different in some cases. In this model, the Douglas tensor is zero; thus, Eq. (47) indicates that the deviation curvature (i.e., J-stability) is constant during the catastrophic shift. In general, the J-stability of the system is not constant during the catastrophic shift when the system includes terms higher than second-order.

Acknowledgments

References

Abolghasem, H. [2012a] "Liapunov stability versus Jacobi stability," *JDSGT* **10**, 13–32.

Abolghasem, H. [2012b] "Jacobi stability of circular orbits in central forces," *JDSGT* **10**, 197–214.

Abolghasem, H. [2013a] "Stability of circular orbits in Schwarzschild spacetime," *IJDSDE* **12**, 131–147.

Abolghasem, H. [2013b] "Jacobi stability of hamiltonian systems," *Int. J. Pure Appl. Math.* **87**, 181–194.

Antonelli, P.L., & Kazarinoff, N.D. [1984] "Starfish predation of a growing coral reef community," *J. Theor. Biol.*, **107**, 667-684.

Antonelli, P.L. [1985] *Mathematical essays on growth and the emergence of form*, (University of Alberta Press, Alberta).

Antonelli, P.L., Ingarden, R.S. & Matsumoto, M. [1993] *The theory of sprays and Finsler spaces with applications in physics and biology*, (Kluwer, Dordrecht).

Antonelli,, P.L. & Bucataru, I. [2003] *KCC theory of a system of second order differential equations, in: Handbook of Finsler Geometry*, (Kluwer, Academic Dordrecht).

Antonelli, P.L., Leandro, E.S., & Rutz, S.F. [2014] "Gradient-driven dynamics on Finsler manifolds: the Jacobi action-metric theorem and an application in ecology," *Nonlinear Stud.* **21**, 141–152.

Bathiany, S., Scheffer, M., Van Nes, E. H., Williamson, M. S., & Lenton, T. M. [2018] "Abrupt climate change in an oscillating world," *Sci. Rep.* **8**, 5040.

Boehmer, C.G. & Harko, T., & Sabău, S.V. [2010] "Jacobi stability analysis of dynamical systems-applications in gravitation and cosmology," *ArXiv: 1010.5464*.

Budyko, M. I. [1969] "The effect of solar radiation variations on the climate of the Earth," *Tellus* **21**, 611–619.

Chen, Y., & Yin, Z. [2019] "The Jacobi stability of a Lorenz-type multistable hyperchaotic system with a curve of equilibria," *Int. J. Bifurcat. Chaos*, **29**, 1950062.

Chiba, S. [1998] "A mathematical model for long-term patterns of evolution: effects of environmental stability and instability on macroevolutionary patterns and mass extinctions," *Paleobiology*, **24**, 336–348.

Crafoord, C., & Källén, E. [1978] "A note on the condition for existence of more than one steady-state solution in Budyko-Sellers type models," *J. Atmospheric Sci.*, **35**, 1123–1125.

Crowley, T. J., & North, G. R. [1991] *Paleoclimatology*, (United States).

Donangelo, R., Fort, H., Dakos, V., Scheffer, M., & Van Nes, E. H. [2010] "Early warnings for catastrophic

shifts in ecosystems: comparison between spatial and temporal indicators," *Int. J. Bifurcat. Chaos*, **20**, 315–321.

Douglas, J. [1927] "The general geometry of paths," *Ann. Math.* **29**, 143–168.

Dănilă, B., Harko, T., Mak, M.K., Pantaragphong, P. & Sabău, S.V. [2016] "Jacobi stability analysis of scalar field models with minimal coupling to gravity in a cosmological background," *Adv. High Ene. Phy.* **2016**, p. 26.

Eisenman, I., & Wettlaufer, J. S. [2009] "Nonlinear threshold behavior during the loss of Arctic sea ice," *PNAS*, **106**, 28–32.

Ghil, M., & Childress, S. [1987] "Persistent anomalies, blocking and predictability," *Topics in Geophysical Fluid Dynamics: Atmospheric Dynamics, Dynamo Theory, and Climate Dynamics*, (Springer, New York), pp. 125–201.

Gilmore, R. [1981] *Catastrophe theory for scientists and engineers*, (Dover, New York).

Gupta, M. K., & Yadav, C. K. [2017] "Jacobi stability analysis of Rössler system," *Int. J. Bifurcat. Chaos*, **27**, 1750056.

Harko, T., Pantaragphong, P., & Sabău, S.V. [2016] "Kosambi-Cartan-Chern (KCC) theory for higher-order dynamical systems," *Int. J. Geo. Meth. Mod. Phy.* **13**, 1650014.

Hutchinson G.E. [1948] "Circular causal systems in ecology," *Ann. NY Acad. Sci.* **50**, 221–246.

Iooss, G., & Joseph, D. D. [1980] *Elementary stability and bifurcation theory*, (Springer-Verlag, Berlin).

Kéfi, S., Dakos, V., Scheffer, M., Van Nes, E. H., & Rietkerk, M. [2013] "Early warning signals also precede non-catastrophic transitions," *Oikos* **122**, 641–648.

Komuro, M. [2002] *Dynamical system*, (SAIENSU-SHA Co.,Ltd., Tokyo).

Lake, M.J. & Harko, T. [2016] "Dynamical behavior and Jacobi stability analysis of wound strings," *Eur. Phys. J.* **76**, 1–26.

Li, Z. X., Ide, K., Le Treut, H., & Ghil, M. [1997] "Atmospheric radiative equilibria in a simple column model," *Clim. Dyn.*, **13**, 429–440.

Ludwig, D., Jones, D. D., & Holling, C. S. [1978] "Qualitative analysis of insect outbreak systems: the spruce budworm and forest," *J. Anim. Ecol.*, **47**, 315–332.

May, R. M. [1977] "Thresholds and breakpoints in ecosystems with a multiplicity of stable states," *Nature*, **269**, 471.

Mirollo, R. E., & Strogatz, S. H. [1990] "Jump bifurcation and hysteresis in an infinite-dimensional dynamical system of coupled spins," *SIAM J. APPL. MATH.*, **50**, 108–124.

Neagu, M. [2013] "Multi-time Kosambi-Cartan-Chern invariants and applications," *BSG Proceedings.* **20**, 36–50.

Roques, L., Chekroun, M. D., Cristofol, M., Soubeyrand, S., & Ghil, M. [2014] "Parameter estimation for energy balance models with memory," *P. ROY. SOC. A-MATH. PHY.*, **470**, 20140349.

Sabău, S.V. [2005a] "Some remarks on Jacobi stability," *Nonlinear Anal. TMA.* **63**, e143–e153.

Sabău, S.V. [2005b] "Systems biology and deviation curvature tensor," *Nonlinear Anal. RWA.* **6**, 563–587.

Saeed, N. A., & El-Gohary, H. A. [2017] "On the nonlinear oscillations of a horizontally supported Jeffcott rotor with a nonlinear restoring force," *NONLINEAR DYNAM.*, **88**, 293–314.

Scheffer, M., Carpenter, S., Foley, J. A., Folke, C., & Walker, B. [2001] "Catastrophic shifts in ecosystems," *Nature*, **413**, 591.

Scheffer, M., Bascompte, J., Brock, W. A., Brovkin, V., Carpenter, S. R., Dakos, V., Held H., Van Nes, E.H., Rietkerk, M., & Sugihara, G. [2009] "Early-warning signals for critical transitions," *Nature*, **461**, 53.

Sellers, W. D. [1969] "A global climatic model based on the energy balance of the earth-atmosphere system," *J. Appl. Meteorol.*, **8**, 392–400.

Strogatz, S.H. [2014] *Nonlinear dynamics and chaos: with applications to physics, biology, chemistry, and engineering*, (Westview press, USA).

Thom, R. [2018] *Structural stability and morphogenesis*, (CRC press, USA).

Udrişte, C. & Nicola, I.R. [2009] "Jacobi stability of linearized geometric dynamics," *J. Dyn. Syst. Geom. Theor.* **7**, 161–173.

Van Nes, E. H., & Scheffer, M. [2007] "Slow recovery from perturbations as a generic indicator of a nearby

catastrophic shift," *Am. Nat.*, **169**, 738–747.

Wang, G., & Zou, X. [2016] "Qualitative analysis of critical transitions in complex disease propagation from a dynamical systems perspective," *Int. J. Bifurcat. Chaos*, **26**, 1650239.

Wright, E. M. [1955] "A non-linear difference-differential equation," *J. Reine Angew. Math*, **194**, 66–87.

Xiang, C., Tang, S., Cheke, R. A., & Qin, W. [2016] "A locust phase change model with multiple switching states and random perturbation," *Int. J. Bifurcat. Chaos*, **26**, 1630037.

Yamasaki, K. & Yajima, T. [2013] "Lotka-Volterra system and KCC theory: Differential geometric structure of competitions and predations," *Nonlinear Anal. RWA.* **14**, 1845–1853.

Yamasaki, K. & Yajima, T. [2016] "Differential geometric structure of non-equilibrium dynamics in competition and predation: Finsler geometry and KCC theory," *J. Dyn. Syst. Geom. Theor.* **14**, 137–153.

Yamasaki, K., & Yajima, T. [2017] "KCC Analysis of the Normal Form of Typical Bifurcations in One-Dimensional Dynamical Systems: Geometrical Invariants of Saddle-Node, Transcritical, and Pitchfork Bifurcations," *Int. J. Bifurcat. Chaos*, **27**, 1750145.

Yoshida, K. [2002] "Long survival of "living fossils" with low taxonomic diversities in an evolving food web," *Paleobiology*, **28**, 464–473.